SrHPO$_4$-coated Mg alloy implant attenuates postoperative pain by suppressing osteoclast-induced sensory innervation in osteoporotic fractures

Guobin Qi [a,1], Zengxin Jiang [a,1], Jialin Niu [b,1], Chang Jiang [c], Jian Zhang [d], Jia Pei [b], Xiao Wang [e], Senbo An [f], Tao Yu [g], Xiuhui Wang [h], Yueqi Zhang [i], Tianle Ma [c], Xiaotian Zhang [j,***], Guangyin Yuan [b,**], Zhe Wang [j,*]

[a] Department of Orthopedics, Shanghai Sixth People's Hospital, Shanghai, 200233, China
[b] National Engineering Research Center of Light Alloy Net Forming and State Key Laboratory of Metal Matrix Composite, Shanghai Jiao Tong University, Shanghai, 200240, China
[c] Department of Orthopedics, Zhongshan Hospital, Fudan University, Shanghai, 200032, China
[d] Shanghai Innovation Medical Technology Co., Ltd, 600 Xinyuan South Road, Lingang New Area, Pudong New District, Shanghai, 201306, China
[e] Department of Orthopedic Surgery, School of Medicine, Johns Hopkins University, Baltimore, MD, 21205, USA
[f] Department of Orthopaedics, Shandong Provincial Hospital Affiliated to Shandong First Medical University, Jinan, 250021, China
[g] Department of Spine Surgery, Guangdong Provincial People's Hospital (Guangdong Academy of Medical Sciences), Southern Medical University, Guangzhou, 510080, China
[h] Department of Orthopedics, Shanghai University of Medicine & Health Sciences Affiliated to Zhoupu Hospital, Shanghai, 201318, China
[i] Department of Traumatic Surgery, Shanghai East Hospital, School of Medicine, Tongji University, Shanghai, 200092, China
[j] Orthpaedic Trauma, Department of Orthopedics, Renji Hospital, School of Medicine, Shanghai Jiao Tong University, Shanghai, 200127, China

A R T I C L E   I N F O

A B S T R A C T

Osteoporotic fractures have become a common public health problem and are usually accompanied by chronic pain. Mg and Mg-based alloys are considered the next-generation orthopedic implants for their excellent osteogenic inductivity, biocompatibility, and biodegradability. However, Mg-based alloy can initiate aberrant activation of osteoclasts and modulate sensory innervation into bone callus resulting in postoperative pain at the sequential stage of osteoporotic fracture healing. Its mechanism is going to be investigated. Strontium hydrogen phosphate (SrHPO$_4$) coating to delay the Mg-based alloy degradation, can reduce the osteoclast formation and inhibit the growth of sensory nerves into bone callus, dorsal root ganglion hyperexcitability, and pain hypersensitivity at the early stage. Liquid chromatography-mass spectrometry (LC-MS) metabolomics analysis of bone marrow-derived macrophages (BMMs) treated with SrHPO$_4$-coated Mg alloy extracts shows the potential effect of increased metabolite levels of AICAR (an activator of the AMPK pathway). We demonstrate a possible modulated secretion of AICAR and osteoclast differentiation from BMMs, which inhibits sensory innervation and postoperative pain through the AMPK/mTORc1/S6K pathway. Importantly, supplementing with AICAR in Mg-activated osteoclasts attenuates postoperative pain. These results suggest that Mg-induced postoperative pain is related to the osteoclastogenesis and sensory innervation at the early stage in the osteoporotic fractures and the SrHPO$_4$ coating on Mg-based alloys can reduce the pain by upregulating AICAR secretion from BMMs or preosteoclasts.

---

* Corresponding author. Orthpaedic Trauma, Department of Orthopedics, Renji Hospital, School of Medicine, Shanghai Jiao Tong University, 160 Pujian Road, Shanghai, 200127, China.
** Corresponding author. National Engineering Research Center of Light Alloy Net Forming and State Key Laboratory of Metal Matrix Composite, Shanghai Jiao Tong University, 800 Dongchuan Road, Minhang District, Shanghai, 200240, China.
*** Corresponding author. Orthpaedic Trauma, Department of Orthopedics, Renji Hospital, School of Medicine, Shanghai Jiao Tong University, 160 Pujian Road, Shanghai, 200127, China.
 E-mail addresses: zhangxiaotian@renji.com (X. Zhang), gyyuan@sjtu.edu.cn (G. Yuan), wangzhe@renji.com (Z. Wang).
[1] These authors contributed equally to this work.

1. Introduction

Osteoporotic fractures, also known as fragility fractures, have become a common public health problem in aggravated geriatric communities, leading to considerable health burden and economic costs [1]. Osteoporotic fractures are usually accompanied by chronic pain [2,3], which mainly involves nociceptive and neuropathic pain and is generally not well controlled [4]. Recent investigations into the mechanisms of pain associated with osteoporotic fractures reveal growing evidence that osteoclasts are not only responsible for bone degradation during the healing process but also closely linked to the nervous system. This highlights the importance of osteoclasts in chronic pain and related neuropathologic conditions, offering a novel perspective for advancing research on pain management following osteoporotic fractures.

The crucial balance between osteoblastic and osteoclastic activity is under the control of many local and general factors in healthy bone, but in osteoporosis, osteoclastic activity is prominent. As previously reported, osteoclast activity is reported to be highly relevant to pain-related issues, including cancer induced bone pain [5], spine pain [6], inflammatory osteolysis [7], and osteoporotic pain [8]. As pain is generally attributed to nociceptors, specialized sensory neurons activated by noxious stimuli [9], sensory innervation might play an essential role between osteoclasts and postoperative pain in osteoporotic fractures. Wang et al. [10] found that osteoclast-initiated porosity of endplates and sensory innervation were associated with low back pain. Zhu et al. [11] found that an increase in osteoclasts in early OA was strongly related to the appearance and persistence of sensory nerves in the subchondral bone, with evidence for a role of osteoclast-derived netrin-1 in mediating OA pain. Previous studies suggested that, following bone fracture, ectopic sprouting of sensory/sympathetic nerve fibers occurs in the callus at most fracture sites, even in those undergoing normal healing [12,13]. However, the ectopic nerve sprouting is not pruned back and generates a neuropathic pain state under certain conditions such as unhealed bone fracture [14], bone cancer [15], osteoarthritis [16], and degenerated vertebral disc [17], as a result of the specific neurotrophic factors secreted by aberrantly-activated osteoclasts in such pathologies, including netrin-1 [11], sema4D [18], and slit3 [19]. Together, these studies indicate that osteoclast-mediated sensory nerve innervation might play an essential role in physiopathology of postoperative pain in osteoporotic fractures.

Mg and Mg-based alloys have been considered as next-generation orthopedic implants for their excellent osteogenic inductivity, biocompatibility, and biodegradability [20–22]. Nevertheless, several issues remain to be addressed before the clinical applications of biodegradable Mg alloy-based orthopedic implants, such as the high rate of corrosion in physiological environments and hydrogen evolution, which result in premature failure of the implant and adverse effects on bone fracture healing. The preparation of coatings on Mg/Mg-based alloys has been used for controllable corrosion rate and hydrogen gas production because it displays sustainable biomechanical properties. Strontium hydrogen phosphate ($SrHPO_4$) coating, which contains strontium (Sr) as the component of coating, was reported to be feasible for osteosynthesis by Mg-based internal fixation in a normal fracture model in our previous study [23]. Strontium ranelate (SrRan), a drug usually prescribed to treat osteoporosis by inhibiting the osteoclast activity, has shown effects of decreasing back pain of osteoporosis patients [24,25]. However, little studies have researched the exact mechanism. The effect of $SrHPO_4$-coated Mg-based alloys on osteoporotic fractures needs further verification to unveil the *in vivo* essences of osteoclast-mediated sensory nerve innervation, especially in osteoporotic fractures where aberrantly activated osteoclasts might induce neuropathic pain.

In this study, we investigated the effect of Mg alloy and $SrHPO_4$-coated Mg alloy on osteoclastogenesis and the role of osteoclasts on sensory innervation during the osteoporotic fracture-healing process. We found that Mg-induced aberrantly-activated osteoclasts increased the sensory innervation of fracture callus at the early stage of osteoporotic fracture healing, and reduction of osteoclast formation by $SrHPO_4$ coating attenuated postoperative pain at the osteoporotic fracture sites; we found evidence for a role of osteoclast-derived Acadesine (AICAR) in regulating sensory innervation and pain threshold.

2. Methods

2.1. Preparation of intramedullary nail specimens and $SrHPO_4$ coating

The Mg alloy utilized in the present study is a newly developed patented Mg–Nd–Zn–Zr alloy (JiaoDa Bio-Mg; abbreviated as JDBM) from National Engineering Research Center of Light Alloy Net Forming & State Key Laboratory of Metal Matrix Composite, Shanghai Jiao Tong University. The elemental composition of the Mg-Nd-Zn-Zr alloy is provided in Table 1. We used Ti6Al4V alloy, Mg alloy, and $SrHPO_4$-coated Mg alloy as the intramedullary nail (IMN) for internal fixation of the femoral shaft fracture, the composition and characterization of which were reported in our previous study [23]. Briefly, A JDBM alloy ingot was cast at 680 °C by semi-continuous casting with high-purity Mg (≥99.99 %), Zn (≥99.995 %), Mg–25%Nd (impurities ≤0.1 %) and Mg–30%Zr (impurities ≤0.5 %) used as raw materials. The cast alloy was extruded at 350 °C with an extrusion ratio of 60 in air. Intramedullary nails were cut from the extruded rod into samples measuring 25 mm in length and 1.5 mm in diameter, and were subsequently ultrasonically cleaned in acetone and alcohol for 10 min, followed by drying with a stream of nitrogen. To obtain $SrHPO_4$ coating, all specimens were incubated at room temperature for 24 h in a solution of 0.1 M HF. An equal volume of 0.2 M $NH_4H_2PO_4$ solution and 0.2 M $Sr(NO_3)_2$ solution were mixed and the freshly prepared solution with a pH of 5.0 was allowed to stand for 24 h to facilitate the formation of the $SrHPO_4$ coating. In the end, all specimens were sterilized with gamma ray (Co-60) radiation at a dose of 29 kGy after treatment and washing with deionized water and drying for 5 min at 37 °C.

2.2. Animal surgery

All animal surgical procedures were conducted following a protocol approved by the Animal Ethics Committee of Zhongshan Hospital, Fudan University (Shanghai, China). We purchased 8-week-old female Sprague-Dawley (SD) rats from Charles River (Beijing, China) and maintained all animals in the animal facility of Zhongshan Hospital, Fudan University (Shanghai, China). To explore the treatment effect of $SrHPO_4$ coating in osteoporotic fracture, we established a rat model of osteoporosis by ovariectomy and inserted Ti6Al4V implants and coated and uncoated Mg alloy implants, into medullary cavities of the rat femur after fracturing their femoral shaft as previously described [23]. Briefly, 8-week-old female rats were anesthetized with an intraperitoneal injection of ketamine (75 mg kg^{-1}) and xylazine (10 mg kg^{-1}) and received bilateral ovariectomy to remove the ovaries via back incisions. Animals were maintained for 3 months for the development of osteoporosis as previously described [26]. The osteoporosis rats were then anesthetized, the knee and femur were exposed, and a 1.5 mm wide and 25 mm long tunnel was drilled from the patellofemoral groove of the distal femur along the femoral shaft axis; finally, a fracture gap was created in the middle of the femoral shaft using a 0.3 mm-diameter string saw, and the implant was inserted into the medullary cavity from the patellofemoral groove. The rats were housed in an environmentally controlled animal care laboratory after the surgery. In addition, one group of rats implanted with Mg alloy IMNs were injected with AICAR (AMPK agonist, 50 mg kg^{-1} d^{-1}, i.p.), and one group of rats implanted

Table 1
The composition of JDBM alloy.

	Mg	Nd	Zn	Zr	Mn	Si	Cu	Fe
Wt %	Balance	2.1	0.21	0.5	0.009	0.006	0.005	0.002

with SrHPO$_4$-coated Mg alloy IMNs were injected with Compound C (AMPK inhibitor, 10 mg kg^{-1} d^{-1}, i.p.) to observe the effect of activation and inhibition of the AMPK/mTORc1/S6K signaling pathway. The vehicles were dimethyl sulfoxide (DMSO) and the specific dosages of AICAR and Compound C adopted in this study were based on a previous study [27].

2.3. Parameters measured in CatWalk analysis

The CatWalk gait analysis system (Noldus Information Technology) was applied to measure the gait parameters of freely moving rats as described previously [11]. Briefly, the CatWalk instrument includes an enclosed walkway with a glass plate floor, a fluorescent lamp from which light is emitted inside the glass plate and completely internally reflected, a high-speed color video camera, and software to record and assess the gait. Each rat was placed in the CatWalk walkway and allowed to walk freely and traverse from one side to the other of the walkway. Where the rat paws contacted the glass plate, the light was reflected down and was recorded with a high-speed color video camera under the glass plate. Every rat was tested until achieving 3 to 5 complete successful runs. A successful run meant that the animal ran the walkway without any interruption or hesitation. The CatWalk software, v10.6, automatically labeled all areas, and subsequently identified and assigned the areas to their respective paws. The following six parameters generated from the recording of successful runs were analyzed:

1) Pawprint area (complete surface area contacted by the paw during the stance phase); 2) Paw pressure (light intensity, which is the mean brightness of all pixels of the print at maximum paw contact); 3) Swing phase (duration in seconds of no paw contact with the glass plate during a step cycle); 4) Stance phase (duration in seconds of a paw contact with the glass floor during a step cycle); 5) Duty cycle (the percentage of stance duration in the step cycle duration); 6) Stride length (distance between successive contact of the same paw).

2.4. Von Frey test

The 50 % paw withdrawal threshold (PWT) was measured using von Frey test hair. Rats were placed in an elevated Plexiglass cage with metal mesh flooring for 15 min before the exploratory behavior analysis until the animal acclimated and got calm. A modification of the Dixon up-down method was applied to test the hind paw mechanic sensitivity [28,29]. A von Frey hair of fixed bending force (force range ≈ 0.4 g, 0.6 g, 1 g, 2 g, 4 g, 6 g, 8 g, or 15 g) was applied vertically to the surface of the hind paws until it just bent and then maintained in place for 2–3 s. If there was no response to the force, the next higher strength hair was applied up to a maximum force of 15 g. After the first response to the force was observed, tests were performed four more times. The 50 % PWT was determined using the following formula: 50 % PWT $= 10[Xf + k\delta]/10,000$, where Xf is the value of the last von Frey hair used in log units, k is the Dixon value for the last six positive/negative response patterns, and δ is the mean difference between stimuli in log units. The threshold force necessary to elicit withdrawal of the paw (median 50 % withdrawal) was determined on two separate trials, with sequential tests separated by at least 5 min.

2.5. Hot plate test

The hot plate test was performed to assess thermal sensitivity. Rats were kept in their holding cages to acclimatize to the experimental room and then placed on the hot plate meter (Bioseb, Vitrolles, France) at 50 °C. The latency to responses indicative of a painful sensation such as shaking, licking, or jumping of the hind paws was recorded to the nearest 0.1 s. The duration of each test was limited to a maximum cut-off of 25 s to avoid scalds.

2.6. Open field test

To assess the locomotor and exploratory activity, each rat was placed at the center of the open-field arena (80 cm × 80 cm × 40 cm) and allowed to move freely for 15 min. The movements of the rats were recorded using a video camera secured on top of the apparatus and analyzed using Noldus software (Noldus Co., Netherlands).

2.7. Histochemistry, immunohistochemistry, and histomorphometry

At the time of euthanasia, we removed and fixed the rat femora and L4-5 DRG in 10 % neutral-buffered formalin for 48 h and decalcified the femora in 10 % ethylenediaminetetraacetic acid (EDTA, pH 7.4) for 4 weeks at room temperature. The samples were then dehydrated in an ethanol gradient and embedded in paraffin or the optimal cutting temperature compound (Sakura Finetek) after the implants were removed gently. Thereafter, the samples were cut into 4 μm thick slices for TRAP staining which was performed using a standard protocol (Sigma-Aldrich). For immunohistology, we incubated slides with antigen retrieval buffer (ab208572, Abcam) at 100 °C for 1 h and washed them with tris-buffered saline (TBS). For immunohistochemistry, we incubated the sections with 0.3 % H$_2$O$_2$ in TBS for 10 min, then blocked with 1 % goat serum (1:100 dilution, Sigma-Aldrich) for 1 h. The sections were then incubated overnight at 4 °C with primary antibodies to p-AMPK (1:200, #2535, Cell Signaling Technology), CGRP (1:200, ab81887, Abcam), NF-200 (1:200, ab8135, Abcam), P2X3 (1:200, ab10269, Abcam), PGP9.5 (1:200, ab10404, Abcam), and β tubulin (1:200, ab6046, Abcam). For immunohistochemical staining, the sections were incubated with the goat anti-rabbit IgG secondary antibody (Invivogen, San Diego, CA, USA) at room temperature for 1 h. Counterstaining was performed using Mayer's hematoxylin (Dako, Hamburg, Germany). For immunofluorescence staining, sections were incubated with secondary antibodies conjugated with a fluorescence probe (Alexa-Fluor 488 or 546) at room temperature for 1 h while avoiding light. Images were analyzed using the Image-Pro Plus software (version 6.0, Media Cybernetics).

2.8. Retrograde tracing

Eight-week-old female SD rats were used to perform osteoporotic fracture as described above. All rats were anesthetized with ketamine and xylazine 4 weeks after the operation. The fracture site was located, and 2 μL 1,1'-dioctadecyl-3,3,3',3'-tetramethylindocarbocyanine perchlorate (Dil) (5 mg mL^{-1}; Sigma-Aldrich) was injected into the fracture callus tissues using an SGE microvolume syringe with a 23-gauge needle (Sigma-Aldrich). Animals were euthanized by cervical dislocation 2 weeks after retrograde injection, and the lumbar dorsal root ganglia (DRGs) (L4, L5) were isolated for immunofluorescence staining. Six micrometer frozen sections were used, and the Dil signals were inspected under 564 nm excitation with a confocal microscope (FV3000, Olympus).

2.9. Ion release in extract medium

Extract medium was prepared according to ISO 10993–5:200997. Briefly, Ti6Al4V, Mg alloy, and SrHPO$_4$-coated Mg alloy implants were immersed in α-MEM supplemented with 10 % (v/v) FBS (Gibco) and 100 U mL^{-1} penicillin-streptomycin (Gibco) at 37 °C in 5 % CO$_2$-containing humidified atmosphere for 3 days. The ratio of sample surface area to the amount of culture medium was 1.25 cm^2 mL^{-1}. The obtained extract media were collected and preserved at 4 °C for subsequent cell culture.

2.10. Cytotoxicity analysis

The cytotoxicity tests of extract medium were performed using a cell counting kit-8 (CCK-8, Beyotime, China). BMMs were incubated in two

96-well plates (5×10^4 cells mL^{-1}, 100 μL per well) for 24 h to adhere, and then, the culture medium was replaced with 100 μL prepared extract medium supplemented with 50 ng mL^{-1} M-CSF. After 24, 48, and 72 h of cell incubation, the culture medium was replaced with a 110 μL fresh serum-free medium consisting of a 10:1 ratio of serum-free culture medium to CCK-8 solution. The cells were incubated for another 4 h, and the optical density value at the wavelength of 450 nm (OD450) was measured with a microplate reader (Thermo Fisher Scientific, Waltham, MA, USA).

2.11. Preparation of preosteoclasts and osteoclasts and collection of conditioned media

The procedures to prepare preosteoclasts and osteoclasts were performed as described previously [30]. BMMs were extracted from the femur and tibia of 8-week-old C57BL/6J mice and cultured in alpha-minimum essential medium (α-MEM, Gibco) containing 10 % fetal bovine serum (FBS, Gibco), 50 ng mL^{-1} macrophage colony-stimulating factor (M-CSF, R&D), and 100 U mL^{-1} penicillin-streptomycin (Gibco). The medium was changed every 2 days. After 4–5 days in culture, the BMMs were collected and seeded into a 24-well plate (1×10^5 cells per well) or 6-well plate (2×10^5 cells per well) and cultured overnight to adhere. On the following day, the culture medium of BMMs was changed to the medium with 50 ng mL^{-1} M-CSF and 50 ng mL^{-1} receptor activator of nuclear factor kappa-B ligand (RANKL, R&D) for 7 days, in the presence or absence of different extracts. TRAP staining was performed to detect TRAP activities of the cultured preosteoclasts and mature osteoclasts using a commercial kit (Sigma-Aldrich), and the cells with more than three nuclei were recognized as TRAP-positive osteoclasts. To collect conditioned medium (CM) from preosteoclasts and osteoclasts (Oc-CM), BMMs were induced for 7 days with extracts as described above and the serum-containing conditioned media from the preosteoclasts and mature osteoclasts were harvested after centrifugation (2500 rpm for 10 min at 4 °C) and stored at −80 °C.

2.12. DRG neuron culture

We harvested and cultured DRG neurons as previously described [11]. The DRG neuron culture medium was minimum essential medium (MEM) supplemented with 5 % FBS (Gibco), 100 U mL^{-1} penicillin-streptomycin (Gibco), 1X GlutaMAX-I supplement (35050-061, Thermo Fisher Scientific), and antimitotic reagents containing 20 μM 5-fluoro-2-deoxyuridine (F0503, Sigma-Aldrich) and 20 μM uridine (U3003, Sigma-Aldrich). Lumbar DRGs (L4-5) were isolated from 8-week-old mice and digested with 1 mL collagenase A solution (10103578001, Roche) at 37 °C for 90 min followed by incubation with 500 μL 1X TrypLE Express solution (15140-122, Thermo Fisher Scientific) at 37 °C for 30 min. DRGs were then washed in 1 mL prepared culture medium three times and triturated gently, after which the DRG neuron suspension was transferred to another tube while non-dissociated tissues settled down to the bottom of the microfuge. The collected Oc-CM was mixed 1:1 (v/v) with the prepared DRG neuron culture medium for the culture of the DRG neurons. Additionally, some cells were incubated with an AMPK inhibitor, Compound C (10 μmol L^{-1}), or an AMPK activator, AICAR (1 mmol/L) (Sigma-Aldrich), the specific dosages of which were based on previous studies [31].

2.13. Immunocytochemistry

For immunofluorescence staining, cell samples were fixed with 4 % paraformaldehyde for 15 min and permeabilized with 0.3 % Triton X-100 for 15 min followed by antigen blocking with 5 % bovine serum albumin for 1 h at RT. The cell samples were then incubated with a primary antibody against calcitonin gene-related peptide (CGRP) (1:200, ab81887, Abcam) overnight at 4 °C and with a secondary antibody Alexa-Fluor 488-conjugated anti-rabbit IgG (Thermo Fisher Scientific). The fluorescent images were captured using a Leica epi-fluorescence microscope (Leica, Wetzlar, Germany) and the intensity of immunofluorescent staining was quantified using ImageJ software (National Institutes of Health).

2.14. LC-MS metabolomic analysis

To explore the effect of SrHPO$_4$-coated Mg alloy on the metabolomics of osteoclasts, BMMs were incubated on a 6-well plate (2×10^5 cells per well) at 37 °C in 5 % CO$_2$ for 1 day, and the culture medium was replaced with prepared extract medium supplemented with 50 ng mL^{-1} M-CSF and 50 ng mL^{-1} RANKL (n = 8), and the osteoclast-induction extract medium was refreshed every 2 days. After 7 days of incubation, culture supernatants were collected after centrifugation (2500 rpm for 10 min at 4 °C) for LC-MS analysis using a Dionex U3000 UHPLC system coupled to a Q-Exactive mass spectrometer (Thermo Fisher Scientific). The liquid chromatography system was fitted with an ACQUITY UPLC HSS T3 column (100 mm × 2.1 mm, 1.8 μm) and the temperature maintained at 45 °C. The mobile phase was composed of 0.1 % formic acid in water (solvent A) and acetonitrile (solvent B). The flow rate was set at 350 μL/min. The mass spectrometer was operated using electrospray ionization (ESI) while alternating between positive and negative ion modes. The acquired spectra were analyzed using Progenesis QI software version 2.4 (Waters). The KEGG ID of differentially expressed metabolites (DEMs) was used to analyze the pathway enrichment, and the metabolic pathway enrichment results were obtained from KEGG database (https://www.kegg.jp/).

2.15. Microfluidics assay

The microfluidics assay was conducted according to previous studies [11]. Briefly, a standard neuron device (450 μm microgroove barrier, SND450) was placed on Corning No. 1 cover glasses (24 × 40 mm). DRG neurons were loaded at a concentration of 2.5–4.5 million cells per mL on the left side of the neuron device, followed by incubation at 37 °C in a 5 % CO$_2$ incubator for 10 min to allow the cells to adhere. Approximately, 150 μL of culture medium was added to each top well, and the media were allowed to flow through the device for 1 min before filling the bottom wells with conditioned media (150 μL) from monocytes, preosteoclasts, and osteoclasts with or without AMPK pathway regulators (compound C, 10 μmol L^{-1}; AICAR, 1 mmol L^{-1}) added to each well on the right side. The device was incubated for another 2 days, and the DRG neurons and their nerve fibers were subjected to standard immunofluorescence staining. Images of nerve fibers that crossed the microchannels were captured using an Olympus DP71 camera, and the length was quantified using ImageJ software.

2.16. Determination of AICAR concentration in cultured media

We determined the concentration of AICAR in the conditioned media using a commercial ELISA kit (MBS2513992, Mybiosourse) according to the manufacturer's instructions. Conditioned media were prepared as described above. Briefly, BMMs were induced with 50 ng mL^{-1} M-CSF and 50 ng mL^{-1} RANKL and supplemented with extract medium for 7 days. The supernatant was collected to carry out the assay after centrifuging the samples for 20 min at $1000 \times g$ and 4 °C.

2.17. Western blotting

Western blot analyses were conducted on the protein harvested from DRG neurons. Briefly, the cell lysates were centrifuged, and the supernatants were separated using sodium dodecyl sulfate-polyacrylamide gel electrophoresis. The separated protein bands were then transferred to a methanol-activated polyvinylidene fluoride (PVDF) membrane, which was labeled with primary antibodies overnight at 4 °C, followed by

incubation with secondary antibodies for 1 h at room temperature. Finally, we detected the levels of proteins using the enhanced chemiluminescence (ECL) kit (Millipore). We used antibodies recognizing mouse AMPK (1:1,000, D5A2, Cell Signaling Technology), p-AMPK (1:1,000, 40H9, Cell Signaling Technology), mTORc1 (1:1,000, 7C10, Cell Signaling Technology), p-mTORc1 (1:1,000, D9C2, Cell Signaling Technology), p70 S6K (1:1,000, 49D7, Cell Signaling Technology), p-p70 S6K (1:1,000, 9204S, Cell Signaling Technology), CGRP (1:1,000, D5R8F, Cell Signaling Technology), and GAPDH (1:1,000, D16H11, Cell Signaling Technology) to measure the levels of specific proteins in the lysates.

2.18. Real-time quantitative PCR (qPCR) assay

Total RNA was extracted using the TRIzol reagent (Invitrogen), and reverse transcription was performed according to the protocol provided by the manufacturer (Takara, Osaka, Japan). The expression of specific genes was detected using the Bio-Rad C1000 tool (Bio-Rad, Hercules, CA, USA) with SYBR Premix ExTaq II (Takara) and normalized to the expression of the housekeeping gene GAPDH. The primer sequences used for qPCR were as follows: AMPK, 5′-AAAGTGAAGGTGGGCAAGCA-3′ (forward) and 5′-GGCTTTCCTTTTCGTCCAACC-3′ (reverse); mTORc1, 5′-TTCCTGAACAGCGAGCACAA-3′ (forward) and 5′-TGCCAAGACA-CAGTAGCGGA-3′ (reverse); S6K, 5′-GAGCTGGAGGAGGGGG-3′ (forward) and 5′-TTTCCTCCGGTCTGAAAGGC-3′ (reverse); CGRP, 5′-GCTCACCAGGAAGGCATCA-3′ (forward) and 5′-GAAGGCTTCA-GAGCCCACAT-3′ (reverse); GAPDH, 5′-AGGTCGGTGTGAACGGATTTG-3′ (forward) and 5′-TGTAGACCATGTAGTTGAGGTCA-3′ (reverse).

2.19. Statistical analysis

All data are presented as means ± standard deviation. We used the two-tailed Student's t-test for comparisons between two groups, and one-way analysis of variance (ANOVA) or two-way ANOVA with Tukey's post hoc test for multiple group comparisons. The data were analyzed using the GraphPad Prism software. $P < 0.05$ was considered to be significant and is indicated by * or #; $P < 0.01$ is indicated by ** or ##.

3. Results

3.1. SrHPO4 coating attenuates postoperative pain during the osteoporotic fracture healing process

To explore the potential effect of SrHPO$_4$-coated Mg alloy on postoperative pain of osteoporotic fractures, we first constructed a femoral shaft fracture model, which was then fixed by intramedullary nails of Ti6Al4V alloy, Mg alloy, and SrHPO$_4$-coated Mg alloy at 3 months after the establishment of ovariectomy (OVX) model in 8-week-old rats. The footprints of rats were obtained using the CatWalk XT system through the routeway device (Fig. 1A). CatWalk analysis at postoperative 4 weeks (Fig. 1B) showed that the SrHPO$_4$-coated Mg alloy group had a relatively larger print area and intensity of hindfoot, while those of the Mg alloy-treated group were smaller than those of the Ti6Al4V alloy group. CatWalk analysis of gait parameters at 8 weeks and 12 weeks after operation was also performed, and the results of postoperative 8 weeks were consistent with those of postoperative 4 weeks (Fig. S1A). Rats were weighed before analysis (Fig. S1B), and there was no significant difference among the groups at each timepoint. We then examined whether gait anomaly was caused by postoperative pain in all groups. The von Frey test showed that, Mg alloy reduced the paw withdrawal threshold at 4 weeks and 8 weeks after the operation, compared to that of the Ti6Al4V alloy group, while SrHPO$_4$-coated Mg alloy increased the paw withdrawal threshold at each time point (Fig. 1C). The hot plate test assessing thermal sensitivity showed that SrHPO$_4$-coated Mg alloy increased the withdrawal latency (Fig. 1D). Furthermore, the open field

test showed that SrHPO$_4$-coated Mg alloy increased the locomotor and exploratory activity (Fig. 1E and F). Overall, the Mg alloy induced postoperative pain at the early healing process, and the SrHPO$_4$-coated Mg alloy attenuates postoperative pain throughout the osteoporotic fracture healing process.

3.2. SrHPO4 coating alleviates the aberrant activation of osteoclasts and the excessive sensory innervation at the osteoporotic fracture site

To examine the potential role of osteoclasts at fracture sites, we investigated osteoclast activities at each stage of fracture healing (Fig. 2A). Quantitative analysis of the density of TRAP$^+$ osteoclasts showed that the Mg alloy promoted osteoclast formation at the fracture sites at 4 and 8 weeks after operation compared with the Ti6Al4V group, which was reversed by SrHPO$_4$ coating to inhibit osteoclast activity (Fig. 2B).

To investigate whether postoperative pain was mediated by innervation and denervation of sensory nerves at the fracture site, we performed immunofluorescence analysis of CGRP$^+$ (Fig. 2A) sensory nerve fibers in the newly formed bone at the fracture site at 4, 8, and 12 weeks after the operation. The density of CGRP$^+$ sensory nerve fibers showed that Mg alloy promoted the density of CGRP$^+$ sensory nerve fibers at 4 and 8 weeks after the operation, compared with that of the Ti6Al4V alloy group at the fracture sites, which was reversed by SrHPO$_4$ coating to reduce sensory innervation (Fig. 2B). Interestingly, the difference in the density of CGRP$^+$ sensory nerve fibers among all groups was consistent with that of osteoclast activities at each time point, suggesting that sensory nerve and osteoclasts might have temporal and spatial accompaniments.

To validate the increased number of DRG neurons responding to the fracture site through CGRP$^+$ sensory innervation in the newly formed bone, we conducted a retrograde labeling experiment using DiI in rats at postoperative 4 weeks (Fig. 2C). Indeed, the number of CGRP$^+$ neurons labeled with DiI in L4-5 DRG in the Mg alloy group was significantly greater than that in the Ti6Al4V alloy and SrHPO$_4$-coated Mg alloy groups (Fig. 2D). Based on the classification of sensory neurons [32], we further stained for another two markers of nociceptive neurons, NF200 and P2X3, and their staining density was also reduced in the SrHPO$_4$-coated Mg alloy group at 4 weeks after the operation. Staining for PGP9.5 and β tubulin to detect other subsets of neuronal fibers in fracture sites showed minimal alterations (Fig. 2E and F).

Taken together, these findings suggest that Mg alloy induced aberrant activation of osteoclasts and sensory innervation at the early stage of osteoporotic fracture healing, which might account for postoperative pain induced by Mg alloy at the early stage of osteoporotic fracture healing. Likewise, SrHPO$_4$ coating might attenuate postoperative pain by inhibiting osteoclast formation and sensory innervation at the fracture site.

3.3. SrHPO4 coating modulates osteoclast differentiation and secretion of AICAR to inhibit sensory innervation

To examine the effect of different extract media on osteoclast differentiation, we prepared extract media from Mg alloy and SrHPO$_4$-coated Mg alloy after immersion for 3 days. We examined the cell proliferation assay of BMMs treated with Ti6Al4V, Mg alloy, and SrHPO$_4$-coated Mg alloy extracts using the CCK-8 and observed that the ability of cell proliferation was not impaired by implant extracts (Fig. 3A). Mg alloy extracts increased osteoclast differentiation determined by TRAP staining, while SrHPO$_4$-coated Mg alloy extracts had a suppression effect on osteoclast activity (Fig. 3B).

To examine the regulation effect of extracts of Ti6Al4V, Mg alloy, and SrHPO$_4$-coated Mg alloy on axonal growth, we first cultured primary DRG neurons collected from adult mice with different extracts and no significant difference was found among all groups (Fig. 3C and D). Subsequently, we cultured BMMs to differentiate into osteoclasts and
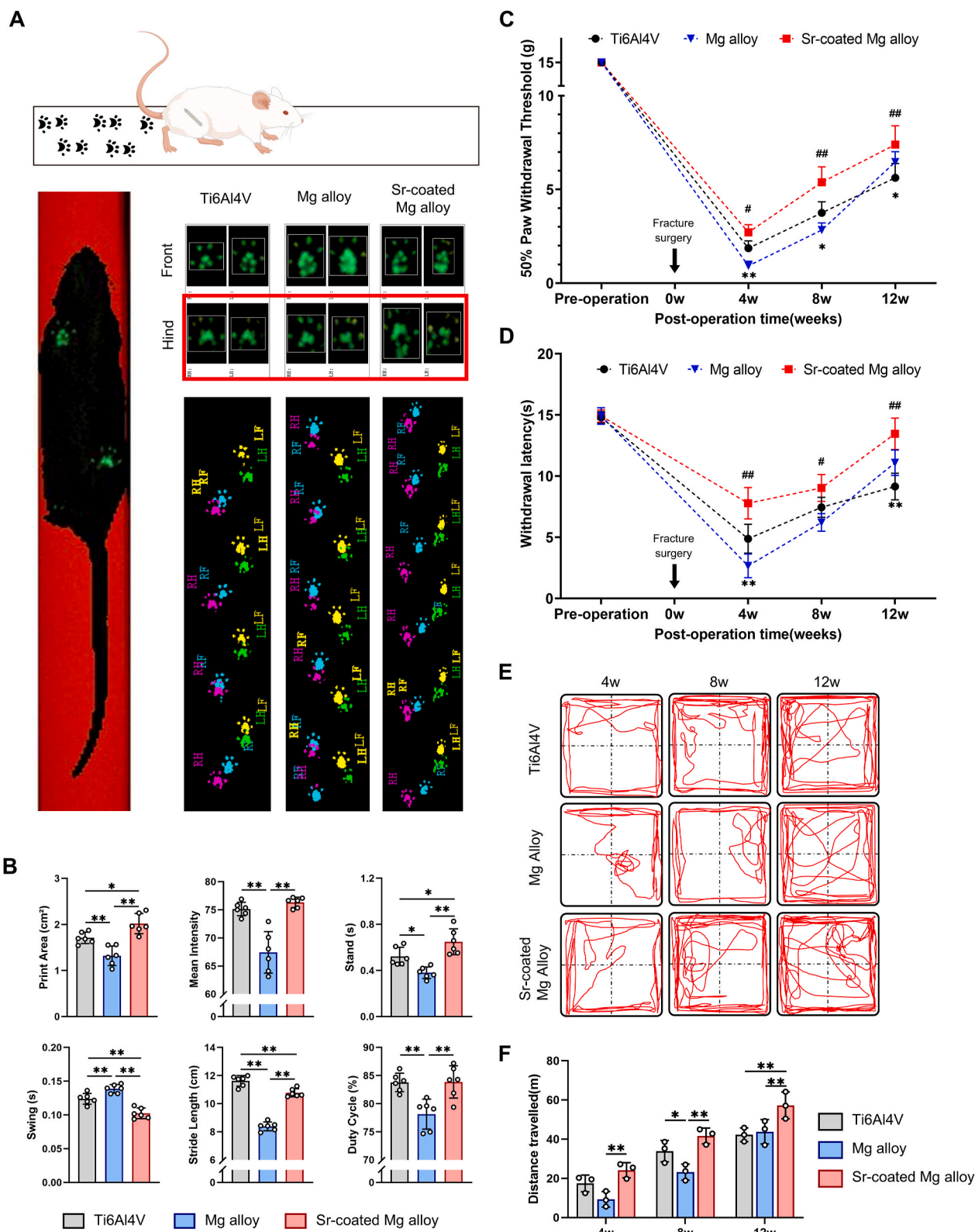
Fig. 1. SrHPO$_4$ coating attenuates postoperative pain during the osteoporotic fracture healing process. (A) Footprints of rats with Ti6Al4V, Mg alloy, and SrHPO$_4$-coated Mg alloy implants obtained using CatWalk XT. (B) Quantitative analysis of variations in the gait parameters of hind limbs at 4 weeks after operation obtained from CatWalk analysis (n = 6). (C) PWT was tested at the hind paw of rats among all groups using von Frey test (n = 6). *p < 0.05, **p < 0.01, Mg alloy vs Ti6Al4V; #p < 0.05, ##p < 0.01, SrHPO$_4$-coated Mg alloy vs Ti6Al4V. (D) The hot plate test was performed at the hind paw of rats to assess thermal sensitivity (n = 6). *p < 0.05, **p < 0.01, Mg alloy vs Ti6Al4V; #p < 0.05, ##p < 0.01, SrHPO$_4$-coated Mg alloy vs Ti6Al4V. (E) Open field test assessing the locomotor and exploratory activity of rats (n = 3). (F) Quantitative analysis of the distance travelled by rats in 15 min. Data are mean ± sd. *p < 0.05, **p < 0.01 using one-way ANOVA (B), or two-way ANOVA (C, D, F) with Tukey's post hoc test.
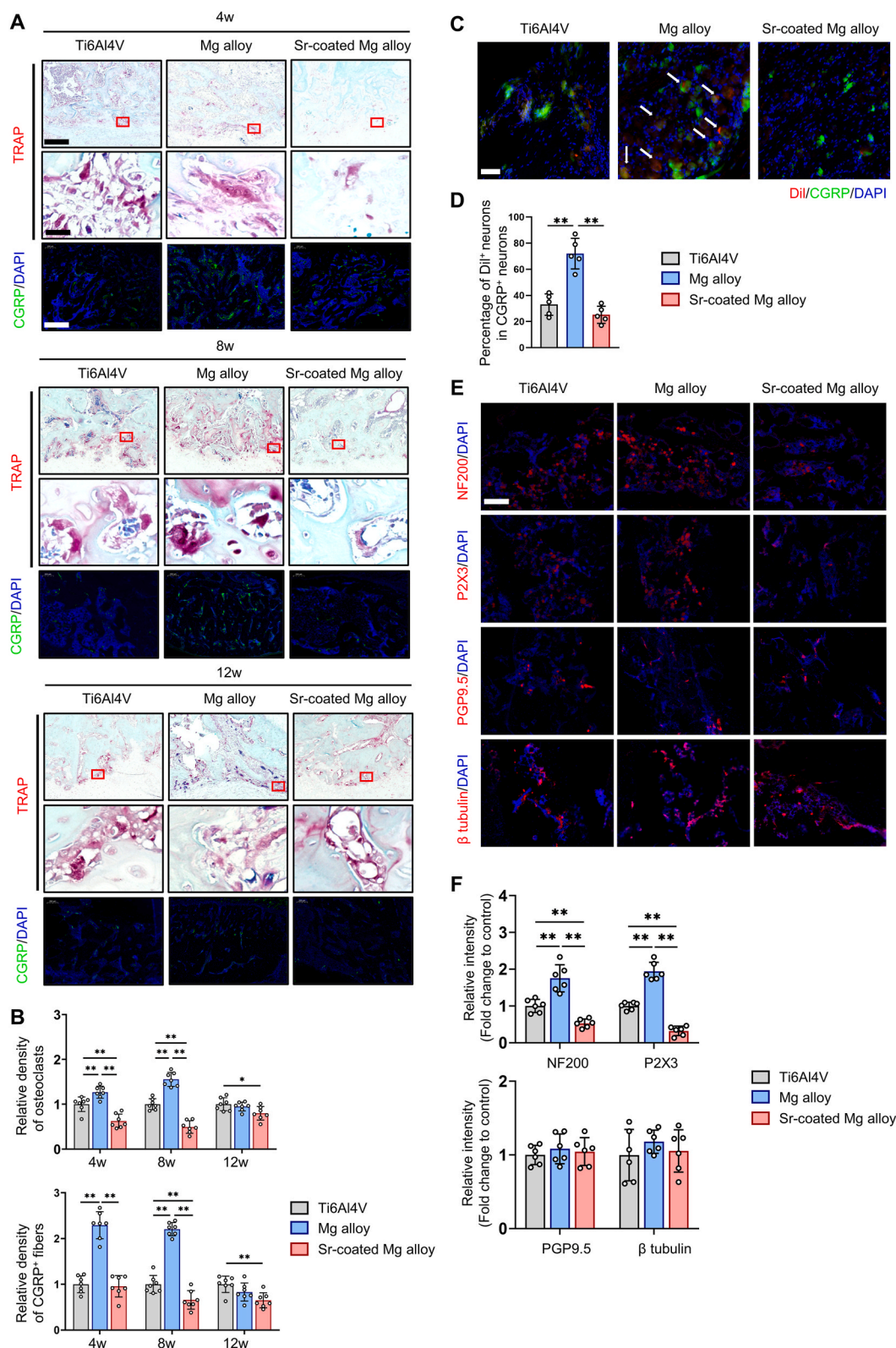
Fig. 2. SrHPO$_4$ coating alleviates the aberrant activation of osteoclasts and the excessive sensory innervation at the osteoporotic fracture site. (A) TRAP staining (top and middle) and immunofluorescence analysis of CGRP$^+$ sensory nerve fibers (bottom, green) at the fracture site at 4, 8, and 12 weeks after operation. Scale bars: 200 μm, 20 μm, and 400 μm, respectively. (B) Quantitative analysis of the relative density of TRAP$^+$ osteoclasts and CGRP$^+$ nerve fibers in newly formed bone. (C) Representative photomicrographs of CGRP and Dil double-labeled neurons in L4 DRG of rats fixed with Ti6Al4V and Mg alloy implants. Scale bar: 100 μm. (D) Percentage of L4 DRG neurons retrogradely labeled with Dil in all CGRP$^+$ neurons at 4 weeks after surgery. (E) immunofluorescence analysis of NF200 (first row), P2X3 (second row), PGP9.5 (third row), and β tubulin (fourth row) at the fracture sites and quantitative analysis of relative intensity. Scale bar, 200 μm. Data are mean ± sd. *p < 0.05, **p < 0.01 using one-way ANOVA (D, F) or two-way ANOVA (B) with Tukey's post hoc test. (For interpretation of the references to color in this figure legend, the reader is referred to the Web version of this article.)
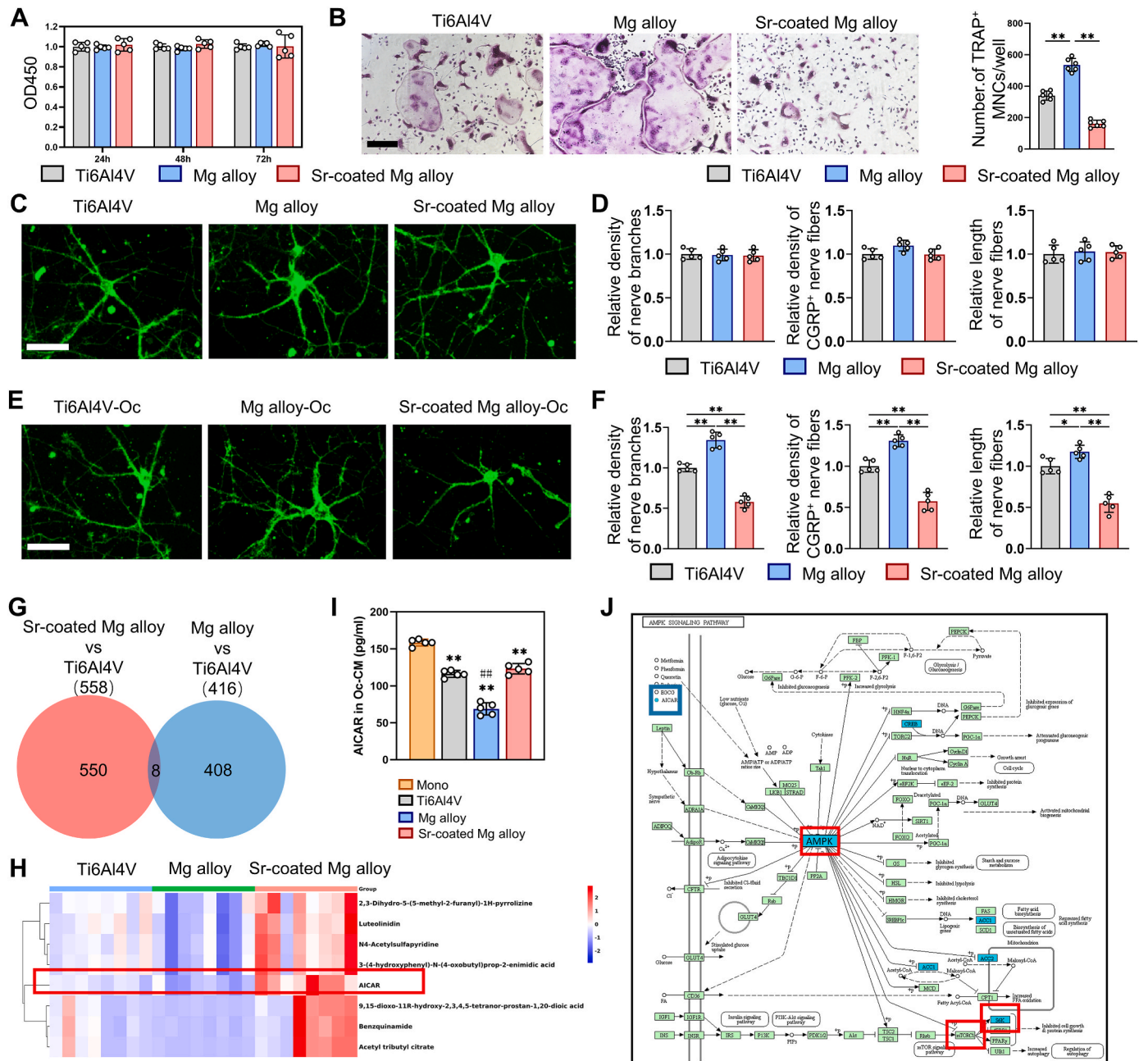
Fig. 3. SrHPO$_4$ coating modulates osteoclast differentiation and secretion of AICAR to inhibit sensory innervation. (A) Cell proliferation assay of BMMs treated with Ti6Al4V, Mg alloy, and SrHPO$_4$-coated Mg alloy extracts using CCK-8. (B) TRAP staining images and quantitative analysis of the number of TRAP$^+$ multinucleate cells (MNCs). Scale bars: 20 μm. (C) Immunocytofluorescence analysis of the effect of implant extracts on nerve fibers. Scale bars: 200 μm. (D) Quantitative analysis of the relative density of nerve branches, and relative length of nerve fibers compared with control group after treatment of different implant extracts. (E) Immunocytofluorescence analysis of the effect of Oc-CM on nerve fibers. Scale bars: 200 μm. (F) Quantitative analysis of the relative density of nerve branches, and relative length of nerve fibers compared with control group after treatment of different Oc-CM. (G) Venn diagram of DEMs in SrHPO$_4$-coated Mg alloy vs Ti6Al4V and Mg alloy vs Ti6Al4V. The 8 DEMs were identified to be upregulated in BMMs by the Sr^{2+} and Mg^{2+} released from SrHPO$_4$-coated Mg alloy and downregulated in BMMs by the Mg^{2+} released from Mg alloy. (H) Heatmap of DEMs, including AICAR, after treatment with different extracts. (I) Concentration of AICAR in Oc-CM treated with different implant extracts. Mono, monocyte-conditioned medium. **p < 0.01 compared with mono group, ##p < 0.01 compared with Ti6Al4V group. (J) Analysis of the AMPK pathway by the KEGG pathways. Data are mean ± sd. *p < 0.05, **p < 0.01 using one-way ANOVA (B, D, F, I) or two-way ANOVA (A) with Tukey's post hoc test.

collected the conditioned media of BMMs and osteoclasts (Oc-CM) to culture primary DRG neurons. Different from the direct culture with extracts, Oc-CM of Mg alloy promoted axonal growth, while Oc-CM of SrHPO$_4$-coated Mg alloy suppressed axonal growth (Fig. 3E and F). Taken together, SrHPO$_4$ coating suppressed axonal growth through the modulation of osteoclast differentiation, but not by directly acting on sensory nerves.

To explore the underlying modulated mechanism of osteoclast activity by SrHPO$_4$-coated Mg alloy on sensory innervation at fracture sites and identify differently expressed metabolites (DEMs), comprehensive metabolomic analysis of Ti6Al4V, Mg alloy, and SrHPO$_4$-coated Mg alloy extract-treated BMMs was performed. Eight DEMs were identified to be upregulated in BMMs by the Sr^{2+} and Mg^{2+} released from the SrHPO$_4$-coated Mg alloy and downregulated in BMMs by the Mg^{2+}

released from the Mg alloy (Fig. 3G). Heatmap of DEMs indicated a difference in the expression of Acadesine (AICAR) after treatment with Ti6Al4V, Mg alloy and SrHPO$_4$-coated Mg alloy extracts (Fig. 3H). AICAR is an agonist of the AMPK pathway, which has been reported previously to be related to CGRP and neuropathic pain [32,33]. To further confirm these observations, we detected the concentration of AICAR in osteoclast-conditioned media and found that it decreased gradually with the differentiation and maturation of osteoclasts (Fig. 3I), indicating that AICAR might derive from BMMs or preosteoclasts. We then performed an analysis of the AMPK pathway by the KEGG pathways and found the AMPK/mTORc1/S6K pathway (Fig. 3J).

Taken together, SrHPO$_4$-coated Mg alloy inhibited osteoclast differentiation and upregulated AICAR secretion from BMMs or preosteoclasts, and therefore had a potential effect on postoperative pain in the osteoporotic fractures.

3.4. AICAR secreted by BMMs/preosteoclasts suppresses axonal growth by activating the AMPK/mTORc1/S6K signaling pathway

To confirm the molecular mechanism by which osteoclasts regulate axonal growth, we cultured primary DRG neurons on the cellular side of a microfluidic culture platform. The wells on the axonal side were filled with different conditioned media. Osteoclast-conditioned media induced growth of axons across the microchannels into the axonal side. However, macrophage/monocyte-conditioned media, the control group, had little effect on axonal growth. Oc-CM of Mg alloy promoted axonal growth, while the supplement of AICAR suppressed axonal growth induced by Oc-CM of Mg alloy. Oc-CM of SrHPO$_4$-coated Mg alloy suppressed axonal growth, while the supplement of Compound C promoted axonal growth inhibited by Oc-CM of SrHPO$_4$-coated Mg alloy (Fig. 4A and B). DRG neurons were also cultured directly with Oc-CM. Quantitative analysis of the relative density of nerve fibers and nerve branches, and relative length of nerve fibers compared with the control group after culturing with Oc-CM represented a consistent trend with the axons that protruded into the axonal side (Fig. 4C and D). To identify the exact effect of AICAR, DRG neurons were cultured with different concentrations of AICAR. Quantitative analysis of the relative density of nerve fibers and nerve branches and relative length of nerve fibers represented a decreasing trend in a concentration-dependent manner (Fig. 4E and F).

To examine the signaling mechanisms of the suppression of axonal growth by AICAR, we tested whether AICAR activated the AMPK pathway of primary DRG neurons. Western blotting showed that AICAR activated the AMPK pathway in a concentration-dependent manner and suppressed the expression of CGRP (Figs. S2A and B). mRNA expression of AMPK, mTORc1, and p70 S6K in DRG neurons treated with Oc-CM showed no significant difference, while the expression of CGRP was significantly suppressed by AICAR (Fig. S2C). Furthermore, we examined the expression of AMPK, p-AMPK, mTORc1, p-mTORc1, p70 S6K, p-p70 S6K, and CGRP using western blotting (Fig. 5A and B) and the expression of AMPK, mTORc1, p70 S6K, and CGRP using qPCR in DRG neurons treated with Oc-CM (Fig. 5C). Oc-CM of Mg alloy promoted the expression of CGRP, while the supplement of AICAR suppressed it. Instead, Oc-CM of SrHPO$_4$-coated Mg alloy suppressed the expression of CGRP, while the supplement of Compound C promoted it. These findings indicated that AICAR secreted by BMMs/preosteoclasts could suppress axonal growth by activating the AMPK/mTORc1/S6K pathway. SrHPO$_4$-coated Mg alloy reduced sensory innervation by inhibiting the formation of osteoclasts and elevated secretion of AICAR.

3.5. AICAR supplementation targeting AMPK/mTORc1/S6K pathway attenuates postoperative pain in Mg-implanted osteoporotic fracture model

To examined whether SrHPO$_4$ coating attenuated postoperative pain in the early postoperative period through the AMPK/mTORc1/S6K pathway, we tested whether activation or suppression of the AMPK

pathway with AICAR (an agonist of the AMPK pathway) and Compound C (inhibitor of the AMPK pathway) could reverse the effect of Mg alloy and SrHPO$_4$-coated Mg alloy on postoperative pain at an early stage of osteoporotic fracture healing. We performed the CatWalk analysis at 4 weeks after the operation, and the footprints of rats were obtained using the CatWalk XT system when they walked through the routeway (Fig. 6A). The quantitative analysis of the gait parameters of hind limbs (Fig. 6B) showed that SrHPO$_4$-coated Mg alloy group had a relatively larger print area than that of the Mg alloy group, suggesting that SrHPO$_4$-coated Mg alloy attenuated the postoperative pain. Interestingly, the effect of Mg alloy and SrHPO$_4$-coated Mg alloy was reversed by activation or suppression of the AMPK pathway. Briefly, Mg alloy + AICAR group attenuated the postoperative pain induced by Mg alloy, and the SrHPO$_4$-coated Mg alloy + Compound C group showed aggravated postoperative pain compared with that in the SrHPO$_4$-coated Mg alloy group. We also performed the von Frey test to assess the postoperative pain, finding that the Mg alloy + AICAR group increased the paw withdrawal threshold compared with that of the Mg alloy group, and the SrHPO$_4$-coated Mg alloy + Compound C group decreased the paw withdrawal threshold compared with that of the SrHPO$_4$-coated Mg alloy group at 4 and 8 weeks after the operation (Fig. 6C).

To examine the effect of the AMPK/mTORc1/S6K pathway on osteoclast and sensory nerve, we performed immunohistochemical analysis of TRAP$^+$ osteoclasts and immunofluorescence analysis of CGRP$^+$ sensory nerve fibers (Fig. 6D) in the newly formed bone at the fracture site 4 weeks after the operation. Quantitative analysis of the density of TRAP$^+$ osteoclasts and CGRP$^+$ nerve fibers (Fig. 6E) showed that SrHPO$_4$-coated Mg alloy inhibited osteoclast activity and sensory nerve innervation, and activation of the AMPK pathway inhibited sensory nerve innervation as well. To further examine the effect of the AMPK/mTORc1/S6K pathway, we also performed immunohistochemical analysis of p-AMPK and immunofluorescence analysis of CGRP in L4-5 DRG (Fig. 6F). Quantitative analysis (Fig. 6G) showed that activation of the AMPK pathway inhibited the expression of CGRP. In conclusion, evidence from both the behavioral and histological analyses suggested that SrHPO$_4$-coated Mg alloy attenuated postoperative pain by activating the AMPK signaling pathway and reducing sensory innervation.

4. Discussion

Most biomaterials currently in use for orthopedic applications, including Mg alloys, focus on their osteogenic properties to accelerate fracture healing through radiological and histological observations. Nevertheless, little attention has been devoted to the incidence and mechanism of postoperative pain in previous studies. The undertreatment of postoperative pain may delay or prevent repair and rehabilitation of fractures [34]. Conversely, the early use and load of the fractured bone were shown to enhance the probability of successful bone repair [35], indicating that effective management of pain is essential for early rehabilitation and better functional outcomes of bone healing. We demonstrated that Mg alloy aberrantly activated osteoclasts and increased the sensory innervation of fracture callus at the early stage of osteoporotic fracture healing, which subsequently induced postoperative pain in osteoporotic fractures. SrHPO$_4$ coating on Mg alloy can reduce the osteoclast formation and inhibit the growth of sensory nerves into bone callus, dorsal root ganglion hyperexcitability, and pain hypersensitivity at the early stage.

To the best of our knowledge, studies started a transition toward clinical research of biodegradable Mg alloy-based implants in orthopedic implant applications [36–39]. Xie et al. [40] found alleviation of postoperative pain in patients with medial malleolar fractures using Mg alloy screws with Ca-P coating. Herber et al. [41] used bioresorbable Mg-Zn-Ca screws in medial malleolar fracture fixation, and almost no pain was observed during the postoperative follow-up. These findings are consistent with the results of SrHPO$_4$-coated Mg alloy in our study;
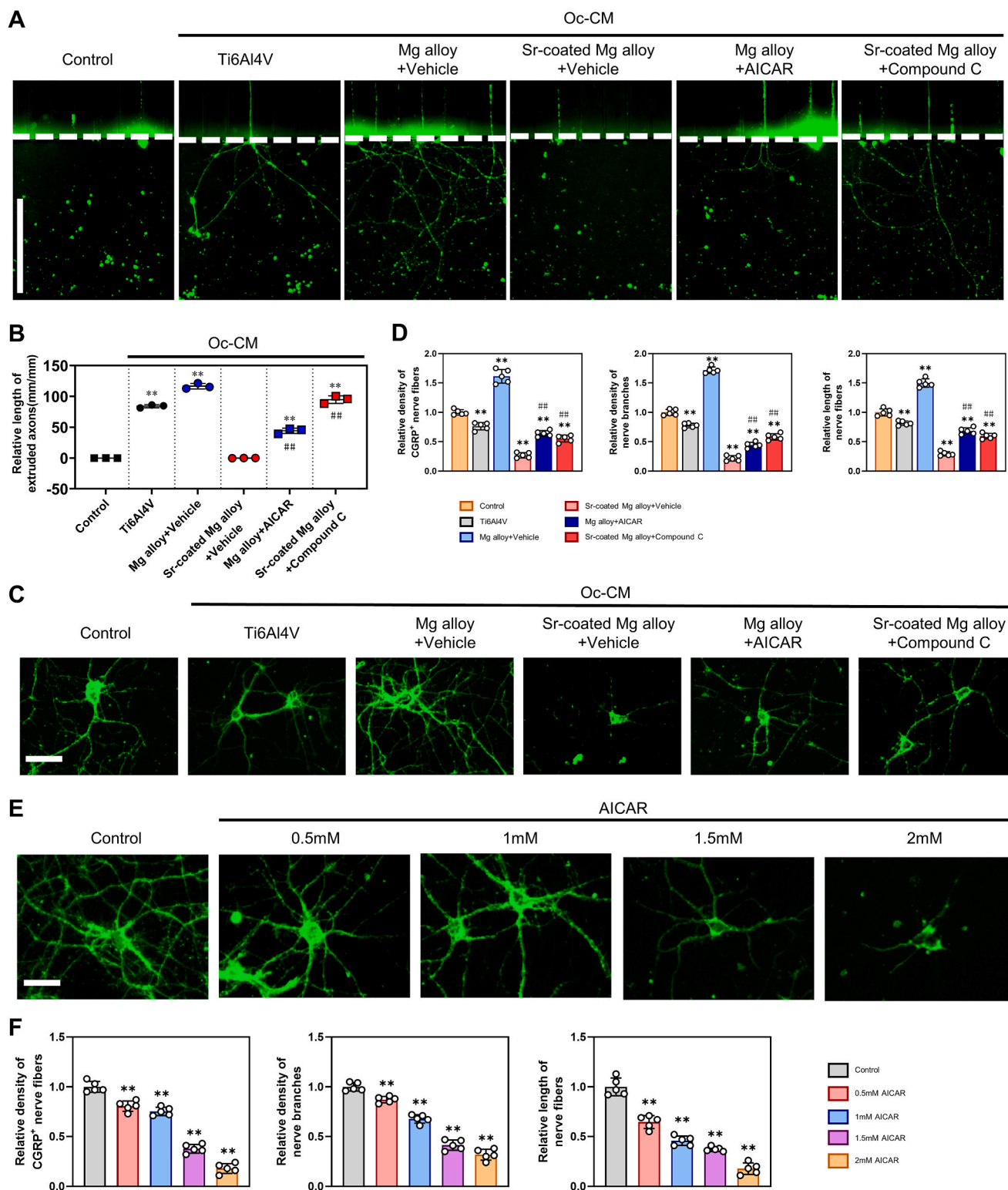
Fig. 4. AICAR secreted by BMMs/preosteoclasts suppresses axonal growth. (A) Microfluidics assay of the effect of osteoclast-conditioned medium obtained after treatment of different implant extracts on DRG neuron axonal growth. Oc-CM, osteoclast-conditioned medium. Scale bar: 100 μm. (B) Quantification of the length of axons that protruded into the axonal side. **$p < 0.01$ compared with the control group; ##$p < 0.01$, Mg alloy + Vehicle vs Mg alloy + AICAR, and SrHPO$_4$-coated Mg alloy + Vehicle vs SrHPO$_4$-coated Mg alloy + Compound C. (C) Immunocytofluorescence analysis of the effect of Oc-CM on nerve fibers. Scale bars: 200 μm. (D) Quantitative analysis of the relative density of nerve fibers and nerve branches and relative length of nerve fibers compared with the control group after treatment of Oc-CM. **$p < 0.01$ compared with the control group; ##$p < 0.01$, Mg alloy + Vehicle vs Mg alloy + AICAR, and SrHPO$_4$-coated Mg alloy + Vehicle vs SrHPO$_4$-coated Mg alloy + Compound C. (E) Immunocytofluorescence analysis of the effect of AICAR on nerve fibers. Scale bars: 200 μm. (F) Quantitative analysis of the relative density of nerve fibers and nerve branches and relative length of nerve fibers compared with the control group after treatment of AICAR. Data are mean ± sd. **$p < 0.01$ using one-way analysis of variance with Tukey's post hoc test.
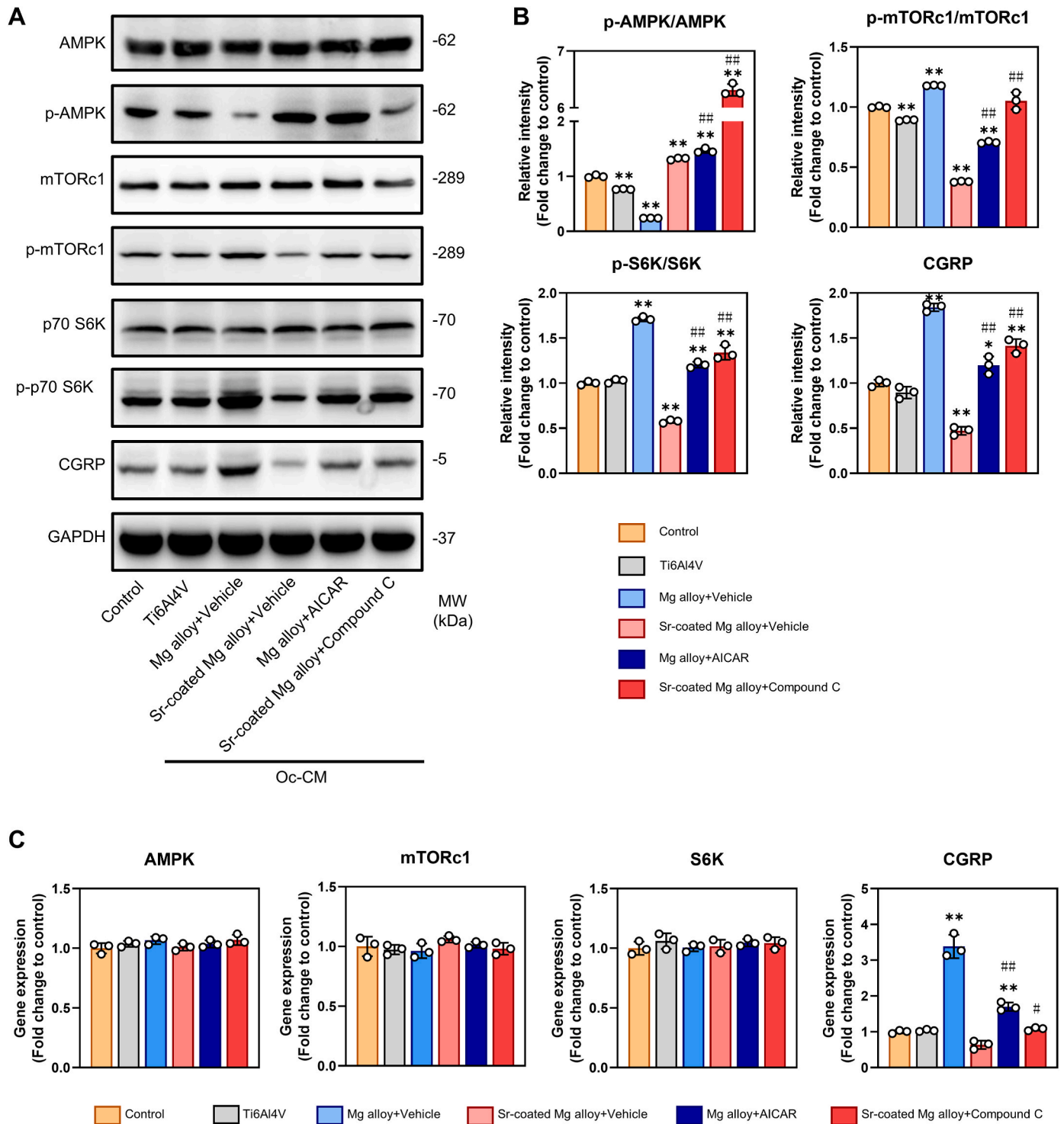
Fig. 5. AICAR secreted by BMMs/preosteoclasts activates the AMPK/mTORc1/S6K signaling pathway. (A) Western blotting of the expression of AMPK, p-AMPK, mTORc1, p-mTORc1, p70 S6K, p-p70 S6K, and CGRP in DRG neurons treated with Oc-CM. (B) Quantitative analysis of p-AMPK/AMPK, p-mTORc1/mTORc1, p-p70 S6K/p70 S6K, and the expression of CGRP in DRG neurons treated with Oc-CM. $*p < 0.05$, $**p < 0.01$ compared with the control group; $\#\#p < 0.01$, Mg alloy + Vehicle vs Mg alloy + AICAR, and SrHPO$_4$-coated Mg alloy + Vehicle vs SrHPO$_4$-coated Mg alloy + Compound C. (C) mRNA expression of AMPK, mTORc1, p70 S6K, and CGRP in DRG neurons treated with Oc-CM. $**p < 0.01$ compared with control group; $\#p < 0.05$, $\#\#p < 0.01$, Mg alloy + Vehicle vs Mg alloy + AICAR and SrHPO$_4$-coated Mg alloy + Vehicle vs SrHPO$_4$-coated Mg alloy + Compound C.

however, the mechanism of reduced pain has not been previously reported. It is not difficult to demonstrate that the Mg alloy implants applied in these clinical trials were meliorated either with surface modification or alloying of other metals, such as Zn, Ca, and Sr. Ca-P coating could both slow down the corrosion rate of Mg alloy [42], and

inhibit osteoclast formation [43,44], which might attenuate postoperative pain in a similar way to SrHPO$_4$ coating. Other components in the alloy, including Zn, Ca, and Sr, also inhibited the osteoclast activity [45–47].

Evidence from both clinical and preclinical studies suggests that
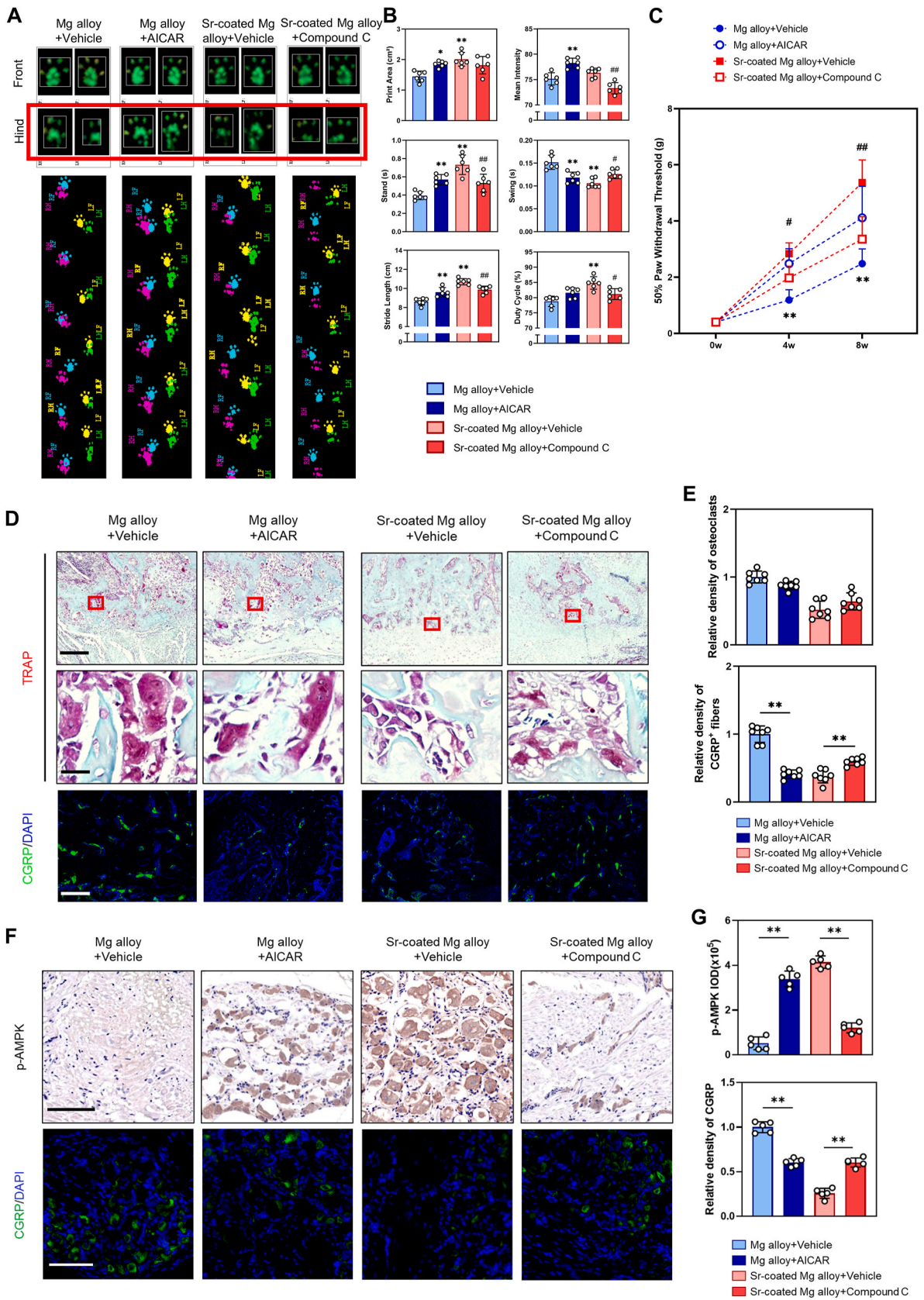
(caption on next page)

Fig. 6. AICAR supplementation targeting AMPK/mTORc1/S6K pathway attenuates postoperative pain in Mg-implanted osteoporotic fracture model. (A) Footprints of rats implanted with Mg alloy + Vehicle, Mg alloy + AICAR, SrHPO$_4$-coated Mg alloy + Vehicle, and SrHPO$_4$-coated Mg alloy + Compound C obtained using CatWalk XT. (B) Quantitative analysis of variations in gait parameters of hind limbs at 4 weeks after surgery obtained from CatWalk analysis (n = 6). *$p < 0.05$, **$p < 0.01$ compared with Mg alloy + Vehicle group; #$p < 0.05$, ##$p < 0.01$ compared with SrHPO$_4$-coated Mg alloy + Vehicle group. (C) PWT was tested at the hind paw of rats (n = 6). **$p < 0.01$, Mg alloy + Vehicle vs Mg alloy + AICAR; #$p < 0.05$, ##$p < 0.01$, SrHPO$_4$-coated Mg alloy + Vehicle vs SrHPO$_4$-coated Mg alloy + Compound C. (D) Immunohistochemical analysis of TRAP$^+$ osteoclasts (top and middle) and immunofluorescence analysis of CGRP$^+$ (bottom, green) sensory nerve fibers in the newly formed bone at the fracture site at 4 weeks after surgery. Scale bars: 200 μm (top), 20 μm (middle), 400 μm (bottom). (E) Quantitative analysis of the relative density of TRAP$^+$ osteoclasts and CGRP$^+$ nerve fibers in newly formed bone. **$p < 0.01$ compared with Mg alloy + Vehicle group; ##$p < 0.01$ compared with SrHPO$_4$-coated Mg alloy + Vehicle group. (F) Immunohistochemical analysis of p-AMPK and immunofluorescence analysis of CGRP$^+$ (green) sensory nerve fibers in L4-5 DRG at 4 weeks after surgery. Scale bars: 100 μm (top), 100 μm (bottom). (G) Quantitative analysis of the expression of p-AMPK and the relative density of CGRP$^+$ sensory nerve fibers. Data are mean ± sd. *$p < 0.05$, **$p < 0.01$ using one-way ANOVA with Tukey's post hoc test. (For interpretation of the references to color in this figure legend, the reader is referred to the Web version of this article.)

osteoclast activity is related to sensory nerves. We also concluded that the aberrant activation of osteoclasts induced by Mg at the fracture site caused more sensory innervation and induced postoperative pain through downregulation of the AICAR/AMPK signaling pathway after Mg alloy fixation. We believe that osteoclast-mediated sensory innervation plays an essential role at the early stage of the osteoporotic fracture-healing process [48,49], and we acknowledge that other mechanisms might be involved in acute bone pain driven by aberrantly-activated osteoclasts, such as acute activation of mechanical and chemical sensitive nociceptors in bone [50], peripheral sensitization by NGF [51], and increased transcription of neurotransmitters including CGRP [52], which is a pain-associated neuropeptide and related to postmenopausal osteoporotic pain [53].

We investigated the molecular mechanisms by which osteoclasts regulated axonal growth and determined that AICAR secreted by BMMs/preosteoclasts suppressed axonal growth by activating the AMPK/mTORc1/S6K signaling pathway. Western blot analysis revealed that Oc-CM from SrHPO$_4$-coated Mg alloy activated the AMPK signaling pathway and downregulated the expression CGRP. However, when we assessed the expression of AMPK, mTORc1, p70 S6K, and CGRP using qPCR in DRG neurons treated with Oc-CM, we found no significant difference in the expression levels of AMPK, mTORc1, and p70 S6K among the three samples. Phosphorylation is essential for the activation of AMPK, which in turn phosphorylates various targets involved in

regulating cellular processes such as metabolism, cell growth, and autophagy. AMPK suppresses the activity of the mammalian target of rapamycin (mTOR), which plays a critical role in promoting cell growth. mTOR is a Ser/Thr protein kinase that acts as a sensor for ATP and amino acids, helping to balance nutrient availability with cell growth. When nutrients are plentiful, mTOR responds to a phosphatidic acid-mediated signal, transmitting a positive signal to p70 S6 kinase. This kinase, a mitogen-activated Ser/Thr protein kinase, is necessary for cell growth and progression through the G1 phase of the cell cycle. In summary, upon activation of the AMPK/mTORC1/p70 S6K signaling pathway, phosphorylation of AMPK, mTORC1, and p70 S6K occurs, although this activation may not be detected through qPCR analysis.

As illustrated in Fig. 7, SrHPO$_4$-coated Mg alloy inhibited osteoclast differentiation and enhanced the secretion of AICAR from BMMs or preosteoclasts. AICAR serves as an agonist of the AMPK pathway, which has been previously reported to be associated with CGRP and neuropathic pain [33]. We demonstrated that SrHPO$_4$-coated Mg alloy reduced sensory innervation and alleviated postoperative pain during the healing process of osteoporotic fractures by activating the AMPK/mTORc1/S6K pathway. Compound C, as an inhibitor of the AMPK pathway, exacerbated postoperative pain in Sr-coated Mg alloy + Compound C group by suppressing the AMPK/mTORc1/S6K signaling pathway (Fig. 6A–C).

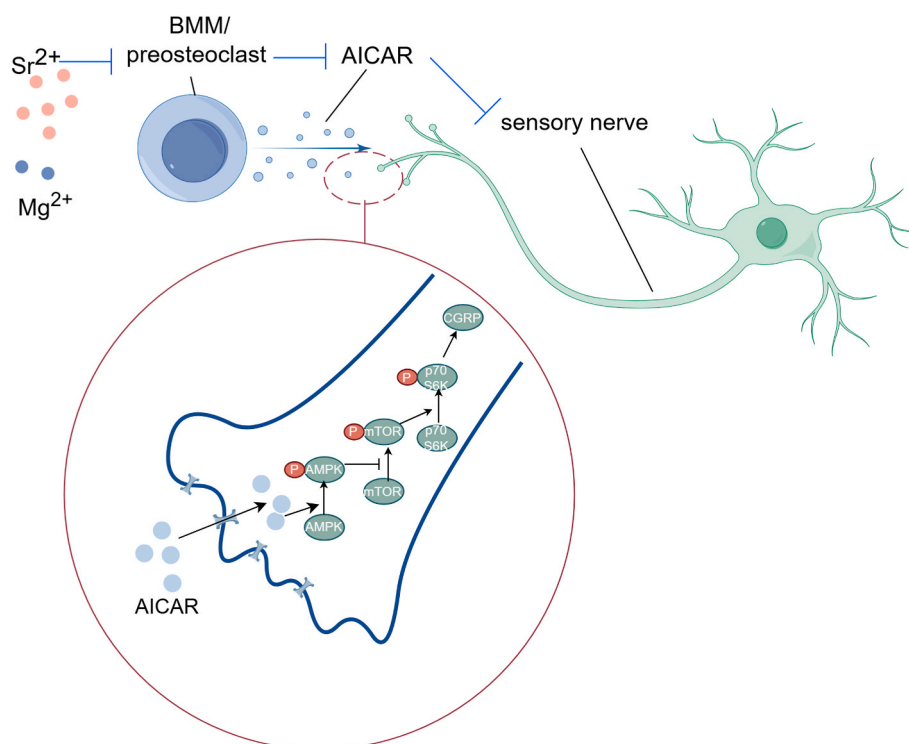Magnesium by itself exerts an effect on sensory nerves. Zhang et al.

Fig. 7. A schematic presentation of the regulatory mechanism of sensory innervation.

[54] identified the role of Mg in promoting CGRP secretion from sensory nerves and CGRP-mediated osteogenesis, while upregulated secretion of CGRP did not cause extra pain 2 weeks after surgery, and no Mg-induced aberrant sprouting of nerve fibers was observed. However, we found that Mg alloy induced postoperative pain by osteoclast-mediated sensory innervation at 4 weeks after operation. Staining of NF200 and P2X3, another two markers of nociceptive neurons, represented significant facilitation of sensory innervation in the Mg alloy group as well (Fig. 2E and F). These results indicate that Mg alloy exerts its effect on postoperative pain probably through osteoclast-mediated sensory innervation at an early stage of osteoporotic fracture healing. Although the inhibition effect of $SrHPO_4$ coating on the expression of CGRP might weaken CGRP-mediated osteogenesis, $SrHPO_4$-coated Mg alloy represented the strongest osteogenesis, probably due to increased osteoblast differentiation and inhibited osteoclast formation by Sr [23].

In this work, we performed an $SrHPO_4$ coating on Mg alloy implants in osteoporotic fractures, which can release Sr^{2+} with degradation and found that $SrHPO_4$ coating attenuated sensory hypersensitivity by inhibiting osteoclastogenesis and sensory innervation, indicating that $SrHPO_4$ coating might be a good analgesic strategy for postoperative pain in patients with osteoporotic fractures.

5. Conclusion

This study revealed an AICAR-mediated mechanism underlying osteoclast-initiated sensory innervation and postoperative pain in osteoporotic fractures fixed by $SrHPO_4$-coated Mg alloy implants. The $SrHPO_4$ coating demonstrated therapeutic potential for alleviating postoperative pain by inhibiting osteoclast differentiation and enhancing the secretion of AICAR to suppress sensory innervation, particularly during the early stages of the osteoporotic fracture healing process. Our study provides a theoretical basis for the future development and clinical application of Mg alloy implants in the treatment of osteoporotic fractures. This is essential for fabricating a coating on Mg substrates to enhance the corrosion resistance of Mg-based implants and to mitigate the potential osteoclast-mediated sensory innervation and postoperative pain induced by Mg. The intervention of the osteoclast differentiation or axonal growth regulator (e.g., AICAR) derived from aberrantly-activated osteoclasts may have therapeutic potential for managing postoperative pain in bone fractures, particularly in osteoporotic fractures.

CRediT authorship contribution statement

Guobin Qi: Writing – original draft, Methodology, Investigation, Data curation, Conceptualization. **Zengxin Jiang:** Writing – original draft, Investigation, Data curation, Conceptualization. **Jialin Niu:** Writing – original draft, Methodology, Investigation, Conceptualization. **Chang Jiang:** Methodology, Investigation. **Jian Zhang:** Resources, Methodology. **Jia Pei:** Methodology, Investigation. **Xiao Wang:** Methodology, Investigation. **Senbo An:** Methodology, Investigation. **Tao Yu:** Methodology, Investigation. **Xiuhui Wang:** Methodology, Investigation. **Yueqi Zhang:** Methodology. **Tianle Ma:** Methodology. **Xiaotian Zhang:** Writing – original draft, Methodology, Conceptualization. **Guangyin Yuan:** Writing – review & editing, Funding acquisition, Conceptualization. **Zhe Wang:** Writing – review & editing, Supervision, Funding acquisition, Conceptualization.

Declaration of competing interest

The authors declare that they have no known competing financial interests or personal relationships that could have appeared to influence the work reported in this paper.

Data availability

Data will be made available on request.

Acknowledgements

Appendix A. Supplementary data

Supplementary data to this article can be found online at https://doi.org/10.1016/j.mtbio.2024.101227.

References

[1] L. Sanchez-Riera, N. Wilson, Fragility fractures & their impact on older people, Best Pract. Res. Clin. Rheumatol. 31 (2017) 169–191.

[2] J.E.M. Sale, L. Frankel, S. Thielke, L. Funnell, Pain and fracture-related limitations persist 6 months after a fragility fracture, Rheumatol. Int. 37 (2017) 1317–1322.

[3] A. Gheorghita, F. Webster, S. Thielke, J.E.M. Sale, Long-term experiences of pain after a fragility fracture, Osteoporos. Int. : A Journal Established as Result of Cooperation Between the European Foundation for Osteoporosis and the National Osteoporosis Foundation of the USA 29 (2018) 1093–1104.

[4] R. Vellucci, et al., Understanding osteoporotic pain and its pharmacological treatment, Osteoporos. Int. 29 (2018) 1477–1491.

[5] J.M. Jimenez-Andrade, et al., Bone cancer pain, Ann. N. Y. Acad. Sci. 1198 (2010) 173–181.

[6] S. Ni, et al., Sensory innervation in porous endplates by Netrin-1 from osteoclasts mediates PGE2-induced spinal hypersensitivity in mice, Nat. Commun. 10 (2019) 5643.

[7] W. Deng, et al., Dendrobine attenuates osteoclast differentiation through modulating ROS/NFATc1/MMP9 pathway and prevents inflammatory bone destruction, Phytomedicine 96 (2022) 153838.

[8] T. Nakagawa, et al., The effects of bisphosphonate on pain-related behavior and immunohistochemical analyses in hindlimb-unloaded mice, J. Orthop. Sci. 23 (2018) 1063–1069.

[9] V. Prato, et al., Functional and molecular characterization of mechanoinsensitive "silent" nociceptors, Cell Rep. 21 (2017) 3102–3115.

[10] Y. Wang, T. Videman, M.C. Battié, ISSLS prize winner, Spine 37 (2012) 1490–1496.

[11] S. Zhu, et al., Subchondral bone osteoclasts induce sensory innervation and osteoarthritis pain, J. Clin. Invest. 129 (2019) 1076–1093.

[12] M. Yasui, et al., Nerve growth factor and associated nerve sprouting contribute to local mechanical hyperalgesia in a rat model of bone injury, Eur. J. Pain 16 (2012) 953–965.

[13] M. Hukkanen, et al., Rapid proliferation of calcitonin gene-related peptide-immunoreactive nerves during healing of rat tibial fracture suggests neural involvement in bone growth and remodelling, Neuroscience 54 (1993) 969.

[14] S.R. Chartier, et al., Exuberant sprouting of sensory and sympathetic nerve fibers in nonhealed bone fractures and the generation and maintenance of chronic skeletal pain, Pain 155 (2014) 2323–2336.

[15] A.P. Bloom, et al., Breast cancer-induced bone remodeling, skeletal pain, and sprouting of sensory nerve fibers, J. Pain 12 (2011) 698–711.

[16] C. Driscoll, et al., Nociceptive sensitizers are regulated in damaged joint tissues, including articular cartilage, when osteoarthritic mice display pain behavior, Arthritis Rheumatol. 68 (2016) 857–867.

[17] S.K. Tolofari, S.M. Richardson, A.J. Freemont, J.A. Hoyland, Expression of semaphorin 3A and its receptors in the human intervertebral disc: potential role in regulating neural ingrowth in the degenerate intervertebral disc, Arthritis Res. Ther. 12 (2010) R1.

[18] G.I. Tasaka, M. Negishi, I. Oinuma, Semaphorin 4D/Plexin-B1-mediated M-Ras GAP activity regulates Actin-based dendrite remodeling through lamellipodin, J. Neurosci. 32 (2012) 8293–8305.

[19] X. Dun, D. Parkinson, Classic axon guidance molecules control correct nerve bridge tissue formation and precise axon regeneration, Neural Regen. Res. 15 (2020) 6.

[20] P. Han, et al., In vitro and in vivo studies on the degradation of high-purity Mg (99.99wt.%) screw with femoral intracondylar fractured rabbit model, Biomaterials 64 (2015) 57–69.

[21] D. Zhao, et al., Current status on clinical applications of magnesium-based orthopaedic implants: a review from clinical translational perspective, Biomaterials 112 (2017) 287–302.

[22] D. Zhao, et al., Vascularized bone grafting fixed by biodegradable magnesium screw for treating osteonecrosis of the femoral head, Biomaterials 81 (2016) 84–92.

[23] Z. Wang, et al., Degradation and osteogenic induction of a SrHPO4-coated Mg–Nd–Zn–Zr alloy intramedullary nail in a rat femoral shaft fracture model, Biomaterials 247 (2020) 119962.

[24] P.D. Delmas, Clinical effects of strontium ranelate in women with postmenopausal osteoporosis, Osteoporos. Int. : A Journal Established as Result of Cooperation Between the European Foundation for Osteoporosis and the National Osteoporosis Foundation of the USA 16 (Suppl 1) (2005) S16–S19.

[25] T.A. Rodrigues, A.J.B. Sampaio Junior, I.D.P. Nunes, M.S.S. Cartágenes, J.B. S. Garcia, Effect of strontium ranelate on pain behavior in an experimental model of osteoarthritis, Braz. J. Med. Biol. Res. 50 (2017) e6314.

[26] S. Chow, et al., Acute inflammatory response in osteoporotic fracture healing augmented with mechanical stimulation is regulated in vivo through the p38-MAPK pathway, Int. J. Mol. Sci. 22 (2021) 8720.

[27] P. Ren, Z. Zhang, P. Wang, H. Zhu, Z. Li, Yangxinkang tablet protects against cardiac dysfunction and remodelling after myocardial infarction in rats through inhibition of AMPK/mTOR-mediated autophagy, Pharm. Biol. 58 (2020) 321–327.

[28] W.J. Dixon, Staircase bioassay: the up-and-down method, Neurosci. Biobehav. Rev. 15 (1991) 47–50.

[29] S.R. Chaplan, F.W. Bach, J.W. Pogrel, J.M. Chung, T.L. Yaksh, Quantitative assessment of tactile allodynia in the rat paw, J. Neurosci. Methods 53 (1994) 55–63.

[30] H. Xie, et al., PDGF-BB secreted by preosteoclasts induces angiogenesis during coupling with osteogenesis, Nat. Med. 20 (2014) 1270–1278.

[31] H. Chen, et al., Berberine attenuates apoptosis in rat retinal Muller cells stimulated with high glucose via enhancing autophagy and the AMPK/mTOR signaling, Biomed. Pharmacother. 108 (2018) 1201–1207.

[32] D. Usoskin, et al., Unbiased classification of sensory neuron types by large-scale single-cell RNA sequencing, Nat. Neurosci. 18 (2015) 145–153.

[33] Y. Yang, et al., Resveratrol suppresses glial activation and alleviates trigeminal neuralgia via activation of AMPK, J. Neuroinflammation 13 (2016) 84.

[34] R.W. Hurley, C.L. Wu, Acute Postoperative Pain, Miller's Anesthesia, 2010.

[35] K.J. Koval, D.A. Sala, F.J. Kummer, J.D. Zuckerman, Postoperative weight-bearing after a fracture of the femoral neck or an intertrochanteric fracture, J. Bone. Joint. Surg. Am. 80 (1998) 352–356.

[36] K. Ding, et al., Titanium alloy cannulated screws and biodegradable magnesium alloy bionic cannulated screws for treatment of femoral neck fractures: a finite element analysis, J. Orthop. Surg. Res. 16 (2021) 511.

[37] M. Li, et al., Titanium alloy gamma nailversus biodegradable magnesium alloy bionic gamma nail for treating intertrochanteric fractures: a finite element analysis, Orthop. Surg. 13 (2021) 1513–1520.

[38] F.C. Wagner, et al., Biodegradable magnesium vs. polylactide pins for radial head fracture stabilization: a biomechanical study, J. Shoulder Elbow Surg. 30 (2021) 365–372.

[39] A. Turan, Y.A. Kati, B. Acar, O. Kose, Magnesium bioabsorbable screw fixation of radial styloid fractures: case report, J. Wrist Surg. 9 (2020) 150–155.

[40] K. Xie, et al., Effectiveness and safety of biodegradable Mg-Nd-Zn-Zr alloy screws for the treatment of medial malleolar fractures, J. Orthop. Transl. 27 (2021) 96–100.

[41] V. Herber, et al., Can hardware removal be avoided using bioresorbable Mg-Zn-Ca screws after medial malleolar fracture fixation? Mid-term results of a first-in-human study, Injury 53 (2022) 1283–1288.

[42] J. Niu, et al., Enhanced biocorrosion resistance and biocompatibility of degradable Mg-Nd-Zn-Zr alloy by brushite coating, Mater. Sci. Eng., C 33 (2013) 4833–4841.

[43] Y.K. Kim, et al., Effect of Ca-P compound formed by hydrothermal treatment on biodegradation and biocompatibility of Mg-3Al-1Zn-1.5Ca alloy; in vitro and in vivo evaluation, Sci. Rep. 7 (2017) 712.

[44] N. Miyatake, et al., Effect of partial hydrolysis of octacalcium phosphate on its osteoconductive characteristics, Biomaterials 30 (2009) 1005–1014.

[45] M. Zaidi, O.A. Adebanjo, B.S. Moonga, L. Sun, C.L. Huang, Emerging insights into the role of calcium ions in osteoclast regulation, J. Bone Miner. Res. 14 (1999) 669–674.

[46] K.H. Park, et al., Zinc inhibits osteoclast differentiation by suppression of Ca^{2+}-Calcineurin-NFATc1 signaling pathway, Cell Commun. Signal. 11 (2013) 74.

[47] B. Kołodziejska, N. Stępień, J. Kolmas, The influence of strontium on bone tissue metabolism and its application in osteoporosis treatment, Int. J. Mol. Sci. 22 (2021) 6564.

[48] S. Mitchell, L.A. Majuta, P.W. Mantyh, New insights in understanding and treating bone fracture pain, Curr. Osteoporos. Rep. 16 (2018) 325–332.

[49] P.W. Mantyh, Mechanisms that drive bone pain across the lifespan, Br. J. Clin. Pharmacol. 85 (2019) 1103–1113.

[50] S. Nencini, et al., Mechanisms of nerve growth factor signaling in bone nociceptors and in an animal model of inflammatory bone pain, Mol. Pain 13 (2016) 1940336997.

[51] F. Denk, D.L. Bennett, S.B. McMahon, Nerve growth factor and pain mechanisms, Annu. Rev. Neurosci. 40 (2017) 307–325.

[52] Y. Niiyama, T. Kawamata, J. Yamamoto, K. Omote, A. Namiki, Bone cancer increases transient receptor potential vanilloid subfamily 1 expression within distinct subpopulations of dorsal root ganglion neurons, Neuroscience 148 (2007) 560–572.

[53] Y. Naito, et al., Alendronate inhibits hyperalgesia and suppresses neuropeptide markers of pain in a mouse model of osteoporosis, J. Orthop. Sci. 22 (2017) 771–777.

[54] Y. Zhang, et al., Implant-derived magnesium induces local neuronal production of CGRP to improve bone-fracture healing in rats, Nat. Med. 22 (2016) 1160–1169.